










ORIGINAL RESEARCH

Angiotensin II Directly Increases Endothelial Calcium and Nitric Oxide in Kidney and Brain Microvessels In Vivo With Reduced Efficacy in Hypertension

Alejandra Becerra Calderon , B.A.Ch; Urvi Nikhil Shroff , PhD; Sachin Deepak, B.S.Ch; Audrey Izuhara , BM; Greta Trogen , B.S.Ch; Alicia A. McDonough , PhD; Susan B. Gurley , MD, PhD; Jonathan W. Nelson , PhD; János Peti-Peterdi , MD, PhD; Georgina Gyarmati , MD, PhD, MPH

BACKGROUND: The vasoconstrictor effects of angiotensin II via type 1 angiotensin II receptors in vascular smooth muscle cells are well established, but the direct effects of angiotensin II on vascular endothelial cells (VECs) in vivo and the mechanisms how VECs may mitigate angiotensin II-mediated vasoconstriction are not fully understood. The present study aimed to explore the molecular mechanisms and pathophysiological relevance of the direct actions of angiotensin II on VECs in kidney and brain microvessels in vivo.

METHODS AND RESULTS: Changes in VEC intracellular calcium ($[Ca^{2+}]_i$) and nitric oxide (NO) production were visualized by intravital multiphoton microscopy of cadherin 5–Salsa6f mice or the endothelial uptake of NO-sensitive dye 4-amino-5-methylamino-2',7'-difluorofluorescein diacetate, respectively. Kidney fibrosis by unilateral ureteral obstruction and Ready-to-use adeno-associated virus expressing Mouse Renin 1 gene (Ren1-AAV) hypertension were used as disease models.

Acute systemic angiotensin II injections triggered >4-fold increases in VEC $[Ca^{2+}]_i$ in brain and kidney resistance arterioles and capillaries that were blocked by pretreatment with the type 1 angiotensin II receptor inhibitor losartan, but not by the type 2 angiotensin II receptor inhibitor PD123319. VEC responded to acute angiotensin II by increased NO production as indicated by >1.5-fold increase in 4-amino-5-methylamino-2',7'-difluorofluorescein diacetate fluorescence intensity. In mice with kidney fibrosis or hypertension, the angiotensin II-induced VEC $[Ca^{2+}]_i$ and NO responses were significantly reduced, which was associated with more robust vasoconstrictions, VEC shedding, and microthrombi formation.

CONCLUSIONS: The present study directly visualized angiotensin II-induced increases in VEC $[Ca^{2+}]_i$ and NO production that serve to counterbalance agonist-induced vasoconstriction and maintain residual organ blood flow. These direct and endothelium-specific angiotensin II effects were blunted in disease conditions and linked to endothelial dysfunction and the development of vascular pathologies.

Key Words: DAF-FM ■ GCaMP6 ■ sex specificity ■ hypertension ■ losartan ■ PD123319 ■ vascular endothelium

Angiotensin II is the classic primary effector of the renin–angiotensin system, and it has multiple vascular and nonvascular sites of actions in various organs to maintain body fluid and electrolyte

homeostasis, effective circulating volume, and blood pressure. Angiotensin II is well known as one of the most potent vasoconstrictors. The molecular signaling pathways mediating the vasoconstrictor actions of

Correspondence to: Georgina Gyarmati, MD, PhD, MPH, Department of Physiology and Neuroscience, Zilkha Neurogenetic Institute, University of Southern California, 1501 San Pablo Street, ZNI 335, Los Angeles, CA 90033. Email: gyarmati.georgina@med.usc.edu

This manuscript was sent to Neel S. Singhal, MD, PhD, Associate Editor, for review by expert referees, editorial decision, and final disposition.

Supplemental Material is available at <https://www.ahajournals.org/doi/suppl/10.1161/JAHA.123.033998>

For Sources of Funding and Disclosures, see page 14.

© 2024 The Authors. Published on behalf of the American Heart Association, Inc., by Wiley. This is an open access article under the terms of the [Creative Commons Attribution-NonCommercial](https://creativecommons.org/licenses/by-nc/4.0/) License, which permits use, distribution and reproduction in any medium, provided the original work is properly cited and is not used for commercial purposes.

JAHA is available at: www.ahajournals.org/journal/jaha

RESEARCH PERSPECTIVE

What Is New?

- Our work reports in vivo validation of the long-established concept that actions of angiotensin II on the vascular endothelium directly counterbalance the simultaneously occurring vascular smooth muscle cell-mediated vasoconstrictions to maintain residual organ blood flow.
- New cell and molecular mechanisms uncovered in this study include diminished angiotensin II-induced vascular endothelial cell calcium and nitric oxide signaling, vascular endothelial cell shedding into the vascular lumen, and microthrombi formation in mouse models of kidney fibrosis and hypertension.

What Question Should Be Addressed Next?

- These results suggest the involvement of altered agonist-induced vascular endothelial cell calcium and nitric oxide responses as likely pathogenic players in endothelial dysfunction and altered hemodynamic responses in hypertensive renal and cardiovascular diseases.

Nonstandard Abbreviations and Acronyms

AT₁R	type 1 angiotensin II receptor
AT₂R	type 2 angiotensin II receptor
AAV	adeno-associated virus
[Ca²⁺]_i	intracellular calcium
DAF-FM	4-amino-5-methylamino-2',7'-difluorofluorescein diacetate
GCaMP	calcium-sensitive green fluorescent protein analog
GEnC	glomerular endothelial cell
GFP	green fluorescent protein
MPM	multiphoton microscopy
NO	nitric oxide
UUO	unilateral ureteral obstruction
VEC	vascular endothelial cell
VSMC	vascular smooth muscle cell

angiotensin II on contractile cell types, such as vascular smooth muscle cells (VSMCs) via the type 1 angiotensin II receptor (AT₁R), and the generally opposite actions via the type 2 angiotensin II receptor (AT₂R) have been well characterized.^{1–3} These include the classic AT₁R-mediated elevations in intracellular calcium ([Ca²⁺]_i) in VSMCs leading to calcium-mediated vasoconstriction.¹

Vascular endothelial cells (VECs) play key roles in the regulation of vascular resistance and organ blood flow. Multilayer intracellular signaling and communication pathways between VECs and VSMCs are known to exist that trigger or regulate endothelium-dependent vasodilation, including increased VEC [Ca²⁺]_i-mediated synthesis of chemical mediators such as nitric oxide (NO), endothelium-dependent hyperpolarization, and myoendothelial coupling.^{4,5} However, the numerous VEC functions, including calcium signaling and NO synthesis, have been difficult to study in vivo due to technical constraints. Only 1 earlier model was established to visualize VEC [Ca²⁺]_i responses in vivo that was limited to studying superficial arterioles.^{6,7} Consequently, angiotensin II-induced VEC calcium signaling has been studied only in vitro in cultured cells⁸ and ex vivo in tissue slices.⁹

Intravital imaging with high-resolution multiphoton microscopy (MPM) has been used successfully to study several vascular and glomerular cell types deep in the intact living kidney including the endothelium.^{10,11} In combination with genetic mouse models with cell-specific expression of fluorescent reporters including the calcium-sensitive GFP (green fluorescent protein) analog (GCaMP) family, MPM imaging has been used to explore cell fate and signaling mechanisms at the single-cell level in great detail in vivo.^{12,13} Therefore, intravital MPM imaging is a state-of-the-art research technique that is ideal for studying endothelial functions in vivo including the direct visualization of the as-yet-unconfirmed effects of angiotensin II on VEC [Ca²⁺]_i and NO signaling.

Vasoconstrictors including angiotensin II are thought to have direct effects on VECs alongside the contractile VSMCs. Endothelial calcium-mediated vasodilatory mechanisms including the actions of angiotensin II on VECs may counterbalance VSMC contractions and act as local feedback inhibitors for agonist-induced vasoconstriction to maintain organ blood flow.^{14–17} While this concept was put forth by several groups in the past, its validity has not been confirmed directly by in vivo imaging.

Several earlier reports have presented conflicting data and views of this concept, providing strong rationale for clarification of the concept. Studies using isolated vessels or VECs cultured in vitro showed that angiotensin II via the AT₁R stimulates calcium signaling and NO production.^{18–20} Increased [Ca²⁺]_i is known as one of the key activating mechanisms of endothelial NO synthase to produce the vasodilator NO.²¹ In addition, angiotensin II is known to activate endothelial NO synthase by stimulating endothelial NO synthase Ser¹¹⁷⁹ phosphorylation and therefore enhance electron flux and calcium sensitivity.¹⁹ However, the opposite results were also reported demonstrating the inhibitory phosphorylation of endothelial NO synthase activity

and reduced NO release from VECs by angiotensin II via AT₁R and thus weakening the vasorelaxant effect of NO on VSMCs to potentiate vasoconstriction.²² Angiotensin II is also known to stimulate the release of endothelin-1, a potent vasoconstrictor.²³ However, these findings were mostly obtained in cell culture, and mechanisms have not been validated in vivo. Finally, chronic vascular diseases and hypertension are known to be associated with high angiotensin II, vascular resistance, VEC dysfunction, and reduced NO production or availability.^{5,24} The presence and role of alterations in angiotensin II-induced VEC calcium signaling in these vascular responses are unknown.

The purpose of the present study was to explore the direct actions of angiotensin II on VEC [Ca²⁺]_i and NO production in vivo in intact kidney and brain microvessels in physiological and disease conditions using direct visual approaches.

METHODS

The data that support the findings of this study are available from the corresponding author upon reasonable request.

Animals

Male and female, 6- to 8-week-old C57BL6/J mice were used in all experiments. Inducible and conditional cadherin 5–Salsa6f fluorescent reporter mice, which specifically express the ratiometric fusion calcium indicator Salsa6f (tdTomato linked to GCaMP6f by a V5 epitope tag) in vascular endothelial cells, were generated by crossing mice expressing Cre-ERT2 recombinase under the control of the cadherin 5 promoter²⁵ (obtained from Cancer Research Technology Limited) and Salsa6f floxed mice²⁶ (Jackson Laboratory, Bar Harbor, ME; Stock No. 031968). Sox2-Salsa6f mice were generated by backcrossing Sox2-Cre²⁷ and Salsa6f floxed mice resulting in ubiquitous expression of the same genetically encoded calcium reporters in all renal cell types. Tamoxifen was administered 75 mg/kg by oral gavage for a total of 3 times (every other day) for full Cre induction in Cre-ERT2 animals. Animals received bolus injection of vehicle or angiotensin II (400 ng/kg, EK-002-12CE; Phoenix Pharmaceuticals, Burlingame, CA) via the cannulated carotid artery alone or in combination with intraperitoneal injection of either AT₁R inhibitor losartan (60 mg/kg), or AT₂R inhibitor PD123319 (25 mg/kg). Eight to 10 mice were allocated to each of the 4 groups (vehicle, angiotensin II, angiotensin II+AT₁Ri, and angiotensin II+AT₂Ri) via simple randomization. The group allocations were available to all the investigators. All animal protocols were approved by the Institutional Animal Care and Use Committee at the University of Southern California.

Adeno-Associated Virus Delivery of Renin to Induce Hypertension

An adeno-associated virus (AAV) construct, AAV8–thyroid hormone-binding globulin–m-Ren1d(F61R/P65S), was used to induce hypertension in cadherin 5–Salsa6f mice as described before.^{28,29} An AAV8–thyroid hormone-binding globulin–GFP construct expressing GFP in target cells was used as the negative control. Both constructs were obtained from Vector Biolabs (Malvern, PA). Animals were randomized into control and hypertensive groups (n=8 mice in each group) 1 week before AAV administration. AAV constructs were suspended in sterile PBS and administered by retro-orbital injection in anesthetized animals at 8 weeks of age (n=8 mice each, 4 males and 4 females each). Renin-AAV dose of 2×10¹⁰ genome copies was used as established earlier.³⁰ Blood pressure was measured 2 times per week for 5 weeks. Plasma renin concentration was measured using ELISA as described before.³¹ In vivo MPM imaging of the brain and kidneys was performed at the end of 5 weeks of follow-up period after hypertension induction. Mice were euthanized after intravital imaging, and brain, kidney, and liver tissues were harvested.

Unilateral Ureteral Obstruction

Unilateral ureteral obstruction (UUO) was performed as described before.³² Briefly, between 6 and 8 weeks of age, the animals were anesthetized with isoflurane, and after a midline laparotomy the left ureter was exposed and ligated 3 times. Successful ligation was confirmed by the hydronephrotic distention of the kidney at the time of imaging (4 weeks after surgery). Control animals underwent sham operation. Ten mice were allocated to each of the 2 groups (control and UUO) via simple randomization.

Intravital or In Vitro Cell Imaging Using MPM

Under continuous anesthesia (isoflurane 1%–2% inhalant via nosecone), mice were placed on the stage of the inverted microscope for kidney or brain MPM imaging. For imaging renal microvessels, the exposed kidney was mounted in a coverslip-bottomed chamber bathed in normal saline as described previously.^{32,33} For MPM imaging of brain arterioles, the forelimb/hindlimb region of the somatosensory cortex was made accessible via a cranial window.³⁴ Briefly, animals were continuously anesthetized with isoflurane and fixed in a stereotaxic frame. After surgical scalp removal, a circular cranial window was drilled and filled with 2% low melt agarose (Sigma) in artificial cerebrospinal fluid and covered with a round glass coverslip. Body temperature was maintained with a homeothermic blanket

system (Harvard Apparatus, Holliston, MA). Alexa Fluor 680-conjugated albumin (Thermo Fisher, Waltham, MA) was administered intravenously by retro-orbital injections to label the circulating plasma (30 μ L IV bolus from 10 μ g/mL stock solution). In some experiments, 4-amino-5-methylamino-2',7'-difluorofluorescein diacetate (DAF-FM) diacetate (Thermo Fisher) was administered intravenously by retro-orbital injection to measure changes in NO production in endothelial cells in vivo.^{35–37} The images were acquired using a Leica SP8 DIVE multiphoton confocal fluorescence imaging system with a 40 \times Leica water-immersion objective (numerical aperture 1.2) powered by a Chameleon Discovery laser at 960 nm (Coherent, Santa Clara, CA) and a DMI8 inverted microscope's external Leica 4Tune spectral hybrid detectors (emission at 510–530 nm for GCaMP6, Fluo-4, and DAF-FM, at 580–640 nm for tdTomato and Fura red, and at 680–740 nm for AF680) (Leica Microsystems, Heidelberg, Germany). The potential toxicity of laser excitation and fluorescence to the cells was minimized by using a low laser power and high scan speeds to keep total laser exposure as minimal as possible. Fluorescence images were collected in volume and time series (xyt, 526 milliseconds per frame) with the Leica LAS X imaging software and using the same instrument settings (laser power, offset, gain of both detector channels). The strong, positive, cell-specific Salsa6f signal (GCaMP6f-tdTomato fluorescence) and high-resolution MPM imaging allowed for easy identification of single VEC cell bodies.

Quantification of Salsa6f, Fluo-4/Fura Red, and DAF-FM Fluorescence Intensities

Optical sections in which long segments of renal or brain microvessels were clearly visible were selected, and time (xyt) series with 1 frame per 526 milliseconds was recorded for 3 to 5 minutes to measure $[Ca^{2+}]_i$ dynamics. The strong, positive signal (Salsa6f or DAF-FM fluorescence) and high-resolution MPM imaging allowed for easy identification of single VEC or VSMC cell bodies. For the quantification of changes in mean Salsa6f ratio (or Fluo-4/Fura red ratio for in vitro glomerular endothelial cell cultures³⁸) or DAF-FM fluorescence intensity,³⁹ region of interest (ROIs) were drawn closely over the total cell body of single cells and the changes in normalized F/F_0 (fluorescence intensity expressed relative to baseline) for DAF-FM or Salsa6f (GCaMP6f/tdTomato ratio) were measured after the experiment in the defined ROI using the Quantify package of LAS X software (3.6.0.20104; Leica-Microsystems). Maximum change in fluorescent intensity was determined by measuring changes in fluorescence intensity at the single-cell level ($n=10$ cells/glomerulus or vessel, $n=10$ glomeruli or vessels/animal, $n=8–10$ animals in each group; $n=4$ frames/

well, and $n=4$ wells/experimental groups in in vitro cell culture studies). Data points represent the average of measurements/animal or culture well.

Blood Pressure and Glomerular Filtration Rate Measurement

Systolic blood pressure was measured by tail-cuff plethysmography (Visitech BP-2000, Visitech System Inc., Apex, NC) in trained conscious animals as previously described.³¹ During acute administration of angiotensin II in anesthetized animals, blood pressure was measured using an analog single-channel transducer signal conditioner model BP-1 (World Precision Instruments, Sarasota, FL) via the carotid artery as described before.^{40,41} Glomerular filtration rate (GFR) measurements were performed using the MediBeacon Transdermal Mini GFR Measurement System (MediBeacon, St. Louis, MO) as described previously.⁴² Briefly, in anesthetized mice, the MediBeacon sensor was placed on the depilated dorsal skin. Mice were injected retro-orbitally with the inulin analog exogenous GFR tracer fluorescein-isothiocyanate conjugated sinistrin (7.5 mg/100 g body weight; MediBeacon). The excretion kinetics of the fluorescein-isothiocyanate conjugated sinistrin was measured for 90 minutes. GFR was then calculated on the basis of the decay kinetics (half-life time) of fluorescein-isothiocyanate conjugated sinistrin using MediBeacon Data Studio software (MediBeacon).

Tissue Processing, Histology, and Immunofluorescence

Immunofluorescence detection of proteins was performed as described previously.³¹ Briefly, organs were perfused and fixed in 4% PFA for 2 hours at room temperature, embedded in paraffin or in optimal cutting temperature compound, and sectioned 8 to 20 μ m thick. For antigen retrieval on paraffin sections, heat-induced epitope retrieval with sodium citrate buffer (pH 6.0) or Tris-EDTA (pH 9.0) was applied. To reduce nonspecific binding, sections were blocked with normal serum (1:20). Primary and secondary antibodies were applied sequentially overnight at 4 $^{\circ}$ C and 2 hours at room temperature. Primary antibodies and dilutions were anti-CD31 (1:100, No. 77699; Cell Signaling Technology, Danvers, MA) and anti-GFP (GFP 1:200; Aves Labs, Davis, CA). Alexa Fluor 488 and 594-conjugated secondary antibodies were purchased from Invitrogen (Waltham, MA) and Jackson ImmunoResearch (West Grove, PA). Slides were mounted by using 4',6-diamidino-2-phenylindole-containing mounting media (VectaShield, Vector Laboratories Inc., Burlingame, CA). Sections were examined with Leica TCS SP8 (Leica Microsystems, Wetzlar, Germany) confocal/multiphoton laser scanning microscope systems as described previously.^{31,43}

Bulk RNA Sequencing and Transcriptome Analysis

Gene expression analysis of AT_{1a}R (Agtr1a), AT_{1b}R (Agtr1b), and AT₂R (Agtr2) in renal vascular endothelial cells was performed using previously published data set (GSE163823).⁴⁴ Data are presented as counts per million transcripts.

RNAscope (mRNA Fluorescence In Situ Hybridization) With Immunofluorescence

AT₁R mRNA detection combined with CD31 immunostaining in mouse kidney sections were manually carried out using the RNAscope Multiplex Fluorescent v2 Assay with TSA Vivid Dyes (323280; Advanced Cell Diagnostics, Newark, CA), and the RNA-Protein Co-Detection Ancillary Kit (323180; Advanced Cell Diagnostics) according to manufacturer's instructions. Briefly, 4 μm formalin-fixed, paraffin-embedded slides were used. RNAscope Co-Detection Target Retrieval reagent was used for antigen-retrieval. Primary (CD31, 77699; Cell Signaling Technology) and secondary antibodies (A11034, Invitrogen), and mRNA Probe- Mm-Agtr1-v2 (406191; Advanced Cell Diagnostics) and RNAscope Multiplex Fluorescent Detection Reagents were applied sequentially. Slides were counterstained with 4',6-diamidino-2-phenylindole and mounted. All slides were imaged using a Leica TCS SP8 (Leica Microsystems) confocal/multiphoton laser scanning microscope system as described previously.^{31,43} Imaris 10.1 Coloc module was used to analyze the percentage of CD31 staining volume colocalized with AT₁R labeling.

GEnC Culture

GEnCs were grown on glass-bottom 6-well plates until reaching a confluent (90%–100%) monolayer using DMEM-based normal GEnC growth media as described previously.³⁸ During experiments, a modified Krebs–Ringer Hco₃ buffer was added to the top of the cells, containing (in mM) 115 NaCl, 5 KCl, 25 NaHco₃, 0.96 NaH₂PO₄, 0.24 Na₂HPO₄, 1.2 MgSO₄, 2 CaCl₂, 5.5 D-glucose, and 100 μmol/L L-arginine. Cells were loaded with the ratiometric calcium dyes Fluo-4 AM and Fura red AM (10 μmol/L each; Invitrogen) dissolved in dimethylsulfoxide at room temperature for ≈20 minutes as described.³⁸ In some experiments, angiotensin II (10^{−9} mol/L) was added to the experimental solution.

Statistical Analysis

Data are expressed as average±SEM and were analyzed using Student's *t* tests or Mann–Whitney test (between 2 groups), or 1-way ANOVA (for multiple groups) with post hoc comparison by Dunnett's multiple comparisons test or Kruskal–Wallis test. Normality

analysis was performed by using the Shapiro–Wilk test. *P*<0.05 was considered significant. There were no animals, data points, or experimental units excluded from the study. Statistical analyses were performed using GraphPad Prism 9.0.1 (GraphPad Software, Inc., La Jolla, CA).

RESULTS

Histological and Functional Features of the Cadherin 5–Salsa6f Mouse Model

Intravital imaging of kidney and brain microvessels (resistance arterioles and capillaries) was performed using MPM in newly established genetic mouse models. To directly and quantitatively visualize changes in [Ca²⁺]_i, specifically in VECs in the intact living kidney cortex and brain, cadherin 5–Salsa6f mice were generated that express the ratiometric fusion calcium indicator Salsa6f (the calcium-sensitive GCaMP6f linked to the calcium insensitive tdTomato) exclusively in the cadherin 5 cell lineage. In addition, Sox2–Salsa6f mice were generated and used to perform [Ca²⁺]_i imaging in all cell types. NO production in VECs was measured using the NO-sensitive fluorescent dye DAF-FM. As illustrated in Figure 1A, this study included in vivo MPM imaging in either physiological conditions or after disease development, and during the systemic administration of an acute angiotensin II challenge (bolus injection of 400 ng/kg angiotensin II into the cannulated carotid artery) with or without pretreatment with either AT₁R or AT₂R inhibitors.

As expected, cadherin 5–Salsa6f mice featured VEC-specific expression of GCaMP6f and tdTomato fluorescent reporters only in the inner layer of blood vessels as demonstrated by in vivo MPM images (Figure 1B) or on the basis of colocalization with the VEC marker CD31 (Figure 1F). Cadherin 5–Salsa6f mice showed no apparent phenotype based on unaltered systolic blood pressure, body weight, and GFR (Figure 1C through 1E).

Intravital MPM Imaging of the Direct Effects of Angiotensin II on VEC Calcium and NO Signaling

Due to the exclusively VEC-specific expression of the genetically encoded calcium reporters, time-lapse intravital MPM imaging of resistance vessels and capillaries in the intact mouse brain and kidney in cadherin 5–Salsa6f mice allowed high-resolution quantitative visualization of the changes in [Ca²⁺]_i, specifically in VECs (Figure 2A and 2B). While the injection of vehicle control had no effect, acute systemic injections of angiotensin II (400 ng/kg into the cannulated carotid artery in bolus) caused instantaneous and substantial

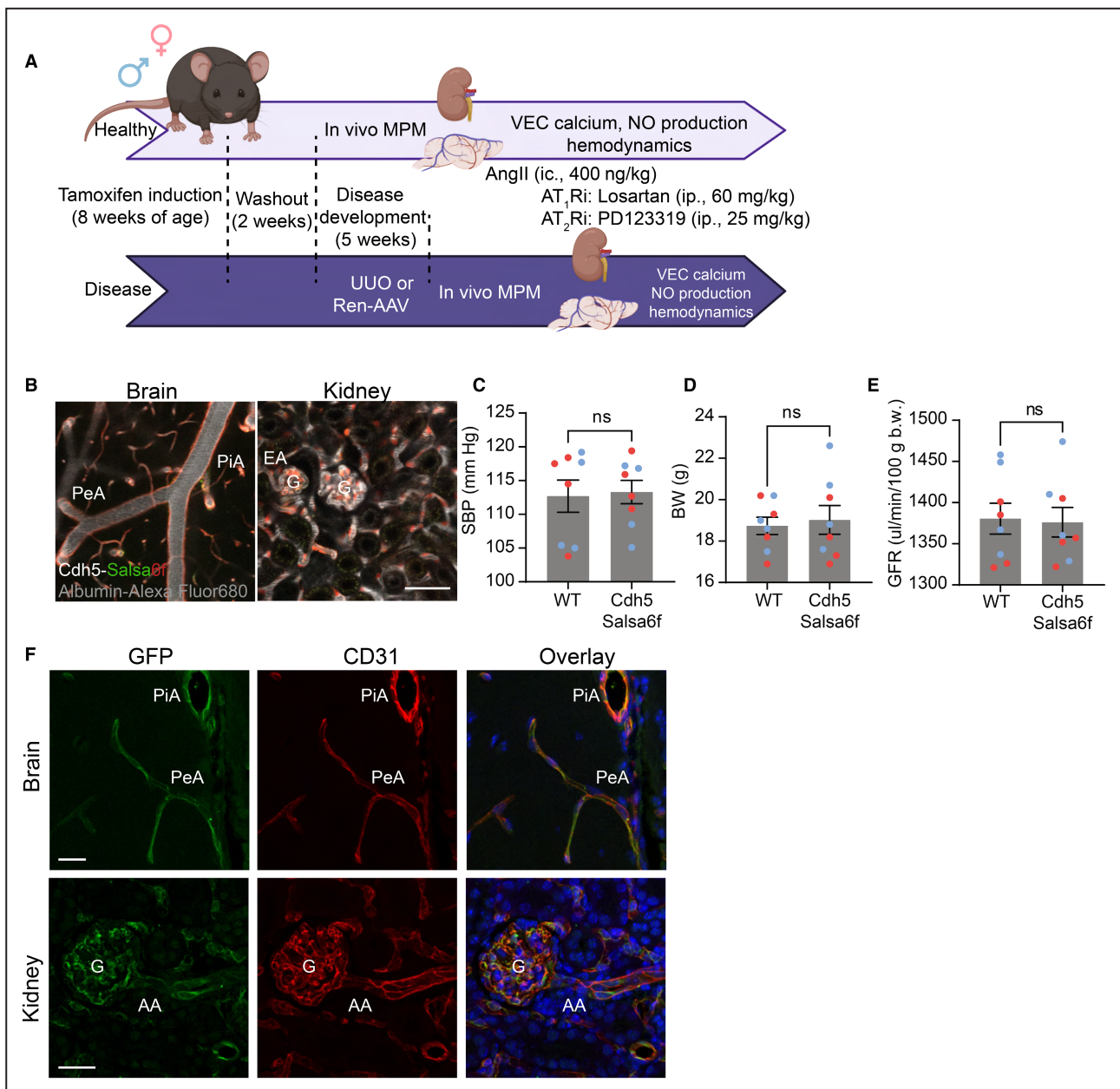


Figure 1. Histological and functional features of the cadherin 5–Salsa6f mouse model.

A, Schematic illustration of the overall study design including the applied physiological and disease in vivo animal models. **B**, Representative in vivo MPM images of intact mouse brain and kidney microvasculature in cadherin 5–Salsa6f animals. Endothelial cells are labeled by the genetic expression of GCaMP6f (green) linked to tdTomato (red). The circulating plasma was labeled by intravenously injected Alexa Fluor 680-conjugated albumin (grayscale). **C** through **E**, Statistical summary of systolic blood pressure (**C**), body weight (**D**), and GFR (**E**) measured in control and cadherin 5–Salsa6f animals at 8 weeks of age. $n=8$ mice each, 4 male (blue) and 4 female (red). **F**, Representative immunofluorescence images of cadherin 5–Salsa6f mouse brain (top) and kidney (bottom) tissue sections demonstrating co-localization of the vascular endothelial cell marker CD31 (red) and the genetically encoded calcium reporter GCaMP6f (green with anti-GFP labeling). Note the complete overlap of CD31 and GFP immunolabeling in the overlay images indicating VEC-specific expression of the Salsa6f reporter. Cell nuclei are labeled blue with 4',6-diamidino-2-phenylindole. Bars are $50\ \mu\text{m}$. AAV indicates adeno-associated virus; AngII, angiotensin II; Cdh5, cadherin 5; EA, efferent arteriole; G, glomerulus; GCaMP, calcium-sensitive green fluorescent protein analog; GFP, green fluorescent protein; GFR, glomerular filtration rate; MPM, multiphoton microscopy; NO, nitric oxide; ns, not significant by Student's *t* test or Mann–Whitney test; PeA, penetrating artery; Pia, pial artery; SBP, systolic blood pressure; UJO, unilateral ureteral obstruction; VEC, vascular endothelial cell; and WT, body weight.

elevations in VEC $[\text{Ca}^{2+}]_i$, both in the brain and kidney on the basis of quantification of the increased Salsa6f signal (Figure 2A and 2B). Video S1 further illustrates

the substantial effects of angiotensin II injection on glomerular VEC $[\text{Ca}^{2+}]_i$. The angiotensin II-induced elevations in VEC $[\text{Ca}^{2+}]_i$ (3.2 ± 0.3 -fold in the brain and

4.6±0.4-fold in the kidney compared with baseline) were completely prevented by pretreatment with the AT₁R inhibitor losartan (1.0±0.1-fold in the brain and 1.2±0.1-fold in the kidney) (Video S1), but not with the AT₂R inhibitor PD123319 (2.6±0.3-fold in the brain and 5.7 ±0.9-fold in the kidney) (Figure 2A and 2B). The potency of the AT₂R inhibitor PD123319 was confirmed on the basis of its significant vasoconstrictor effects in renal resistance arterioles (Figure 2C) after intracarotid injections. These confirmatory studies were performed using young female mice due to the well-known higher expression of the AT₂R in females and its age-dependent decline.⁴⁵ Furthermore, the analysis of previously published bulk RNA expression data of renal endothelial cells⁴⁴ showed detectable expression levels of AT_{1a}R, but minimal or undetectable expression of the AT_{1b}R and AT₂R (Figure 2D). Comparison of the magnitude of the angiotensin II effects on VEC [Ca²⁺]_i in brain (3.2-fold) versus kidney (4.5-fold) microvessels suggested that renal VECs are more responsive to angiotensin II than brain VECs (Figure 2E). Importantly, high temporal resolution MPM imaging revealed that the elevations in VEC [Ca²⁺]_i always preceded angiotensin II-induced vasoconstrictions (Figure 2F). In addition, in vivo MPM imaging of the same brain and renal microvessels was performed in Sox2-Salsa6f mice that feature Salsa6f expression in all cell types. Time-lapse calcium imaging during the same acute angiotensin II challenge confirmed that the elevations in VEC [Ca²⁺]_i always preceded the [Ca²⁺]_i changes of directly adjacent VSMCs (Figure 2F).

Additional MPM imaging studies were performed to measure the changes in VEC NO production in response to the same angiotensin II challenge. The intravenous injection of DAF-FM diacetate specifically labeled the endothelial layer of brain and kidney microvessels as illustrated in Figure 2G. Acute angiotensin II injections caused ≈2-fold increases in VEC NO production in the brain and the kidney compared with baseline (Figure 2G).

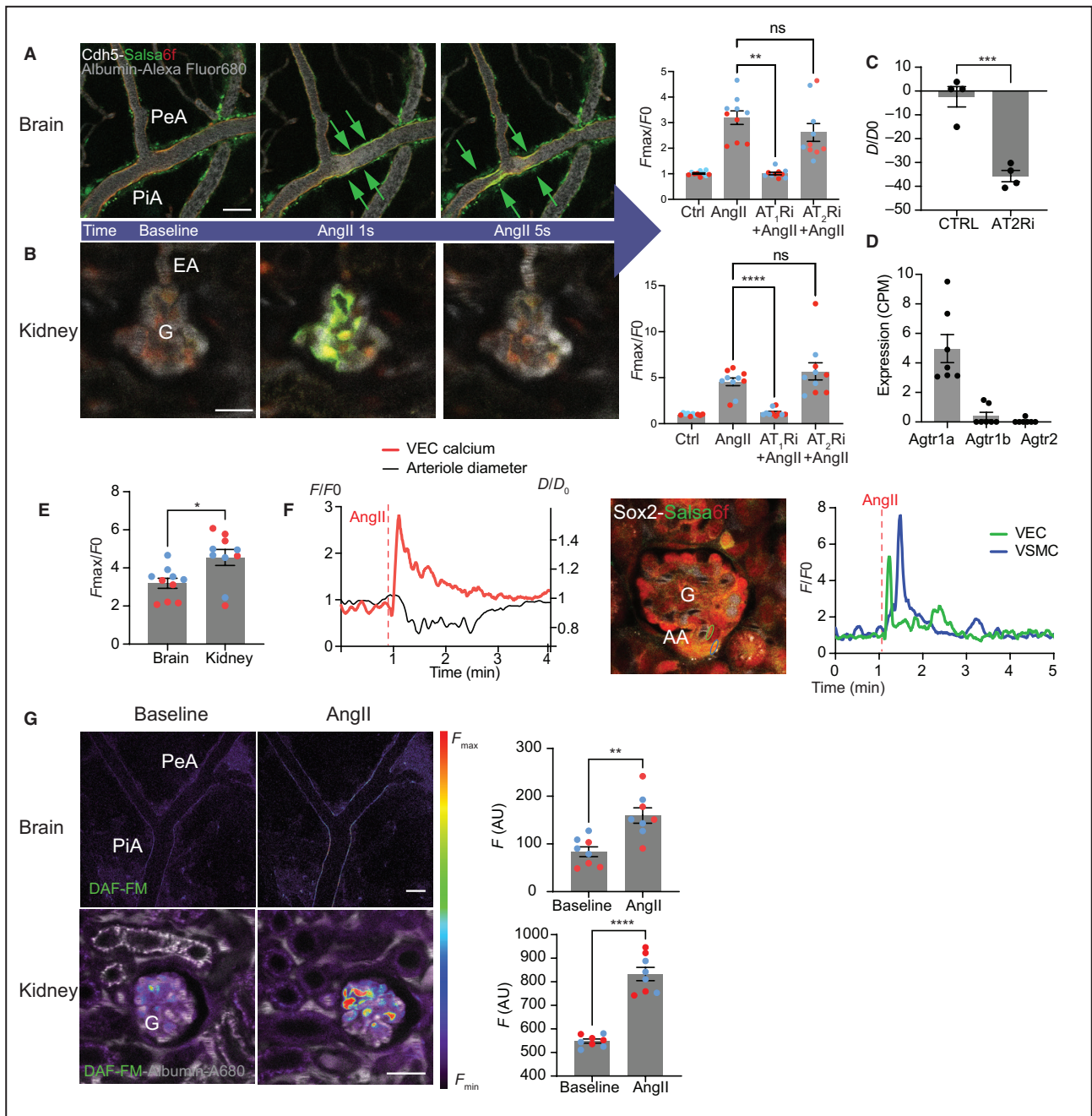
Angiotensin II Effects on Glomerular Endothelial Cells Cultured In Vitro

To further confirm the direct and VEC-specific effects of angiotensin II, GEnCs were cultured in vitro and loaded with either calcium or NO-sensitive fluorescent dyes Fluo-4/Fura red or DAF-FM, respectively. Consistently with the above in vivo effects, the addition of angiotensin II (10⁻⁹ mol/L) to the GEnC culture media caused prompt and significant elevations in GEnC [Ca²⁺]_i and NO production (Figure 3A through 3E). The angiotensin II-induced GEnC [Ca²⁺]_i responses were completely blocked by pretreatment with the AT₁R inhibitor losartan but not with the AT₂R inhibitor PD123319 (Figure 3D).

Diminished Effects of Angiotensin II on Endothelial Cell Calcium and NO Signaling in Disease Conditions

To test for potential alterations in angiotensin II-induced VEC responses in disease conditions, the same acute vasoconstrictor challenge by angiotensin II injection was applied in the UUO renal fibrosis model and under chronic hypertension conditions (Figure 4). The appearance of second harmonic generation signal, which is derived from collagen fibers, confirmed the successful induction of tissue fibrosis (Figure 4C). As observed with in vivo MPM imaging, acute systemic injections of angiotensin II (400 ng/kg IC in bolus) in mice 5 weeks after UUO caused instantaneous and significant elevations in VEC [Ca²⁺]_i measured in the key renal resistance vessels, the afferent arteriole, on the basis of quantification of the increased Salsa6f signal (Figure 4A). However, the magnitude of the angiotensin II-induced VEC [Ca²⁺]_i elevations was significantly reduced in UUO compared with control healthy conditions, resulting in more robust afferent arteriole vasoconstrictions in UUO versus control (Figure 4B). Similarly, acute angiotensin II injections induced detectable elevations in VEC NO production but with a significantly smaller magnitude compared with control (Figure 4C).

In addition, chronic hypertension was established in a separate group of cadherin 5-Salsa6f mice by the systemic injection of Ready-to-use adeno-associated virus expressing Mouse Renin 1 gene (Ren1-AAV), which resulted in sustained high blood pressure in the 150 mmHg range (Figure 5A). GFP-AAV-injected mice served as controls. Ren1-AAV hypertensive mice had substantial elevations in plasma renin concentration (Figure 5B) and renin expression in the liver compared with control mice (Figure 5C), validating the gene delivery and hypertension induction approach. In vivo MPM imaging revealed that acute systemic injections of angiotensin II caused significant elevations in VEC [Ca²⁺]_i measured in brain and kidney microvessels (Figure 5D through 5F). However, the magnitude of the angiotensin II-induced VEC [Ca²⁺]_i elevations was significantly reduced in Ren1-AAV hypertensive mice compared with control healthy conditions. The reduced direct angiotensin II effect on VEC calcium signaling in hypertension resulted in more robust small artery vasoconstrictions and larger blood pressure elevations in response to acute angiotensin II injection in Ren1-AAV mice compared with control (Figure 5G). AT₁R mRNA expression in VECs was not altered in hypertension versus control condition, in contrast to AT₁R upregulation in the glomerular mesangium (Figure 5H), which was previously reported.⁴⁶ Interestingly, the VEC [Ca²⁺]_i responses appeared to be more preserved in female versus male UUO and hypertensive mice (Figures 4B



and 5G). Additional pathologies were observed with in vivo MPM imaging in hypertensive mice, including the angiotensin II-induced formation of microthrombi in both brain and kidney resistance arterioles and the shedding of several VECs into the lumen of glomerular capillaries (Figure 5D and 5F and Video S2).

DISCUSSION

The present work is the first to visualize the effects of angiotensin II directly on vascular endothelial calcium signaling and NO production in intact organs in vivo. As one major outcome of this study, the results provided

in vivo validation of the long-established concept that actions of angiotensin II directly on the vascular endothelium through the synthesis and release of vasodilatory autocooids counterbalance the simultaneously occurring VSMC-mediated vasoconstrictions to maintain residual organ blood flow. We showed that this direct VEC-targeting action of angiotensin II is mediated via AT₁R-dependent calcium signaling and NO generation. As another main outcome, the present work uncovered new cell and molecular mechanisms, diminished angiotensin II-induced VEC calcium and NO signaling, VEC shedding into the vascular lumen, and microthrombi formation in mouse models of kidney

fibrosis and hypertension. These results suggest the involvement of altered agonist-induced VEC calcium and NO responses as likely pathogenic players in endothelial dysfunction and altered hemodynamic responses in hypertensive renal and cardiovascular diseases.

The generation and application of the cadherin 5–Salsa6f mouse model in the present study for intravital MPM imaging of $[Ca^{2+}]_i$ specifically in VECs in the intact brain and kidney resistance arterioles is an innovative technical advance. Cadherin 5–driven expression of the fast and highly sensitive genetically encoded truly ratiometric calcium indicator Salsa6f²⁶ (Figure 1B and 1F) was essential and permitted detection of changes in $[Ca^{2+}]_i$ specifically in VECs. Exemplified by the present experiments (Figures 2, 4, and 5), this new research tool is expected to aid many future studies in vascular biology and disease. In addition to $[Ca^{2+}]_i$, the present study quantitatively visualized VEC NO production in vivo in the kidney and brain using the NO-sensitive fluorescent dye DAF-FM similarly to previous in vivo and in vitro applications in many vascular beds.^{35–37} The brain and kidney were selected for the present imaging studies because these 2 organs are known to have the most robust organ blood flow autoregulation⁴⁷ and which may contribute to pathological conditions such as renal fibrosis and hypertension.

Acute injection of angiotensin II triggered substantial increases in VEC $[Ca^{2+}]_i$ and NO production in resistance arterioles and capillaries in the intact kidney

and the brain in vivo (Figure 2). Although angiotensin II–induced hemodynamic changes, shear stress, and myoendothelial coupling could have caused secondary elevations in VEC $[Ca^{2+}]_i$, the observed responses strongly suggested the direct effects of angiotensin II on VEC calcium signaling and NO production. The results of 3 separate lines of the current investigation support this point: (1) Angiotensin II–induced VEC $[Ca^{2+}]_i$ responses were observed before vasoconstriction (Figure 2F), (2) before VSMC $[Ca^{2+}]_i$ elevations, and (3) were present in isolated in vitro cultured GEnCs (Figure 3). These results provide important in vivo validation of the long-existing concept^{14–17} and confirmation that angiotensin II–induced direct endothelial calcium-mediated vasodilatory mechanisms are present in vivo and may play important roles to counteract vasoconstrictions and maintain organ blood flow. Both in vivo and in vitro studies in the present work found that these angiotensin II effects were mediated via the AT₁R rather than the AT₂R (Figures 2A and 3D). These results are consistent with the functional expression of AT₁R in VECs^{8,14} and with the hypotensive phenotype and the significantly reduced pressor response to acute angiotensin II infusion in mice with VEC-specific expression of a constitutively active AT₁R mutant that were reported earlier.¹⁵ The detectable expression of the AT_{1a} receptor subtype compared with the minimal or undetectable levels of the AT_{1b} and AT₂ receptors in renal VECs in our previously published database⁴⁴

Figure 2. Intravital imaging of the direct effects of angiotensin II on VEC calcium signaling and NO production in the intact mouse brain and kidney microvasculature.

A and B, Representative in vivo MPM images of VEC $[Ca^{2+}]_i$ responses in cadherin 5–Salsa6f mouse brain (**A**) and kidney (**B**) microvessels at baseline and 1 and 5 seconds after intracarotid bolus angiotensin II injection. Note the robust increase in Salsa6f fluorescence intensity within 1 second after angiotensin II injection indicating substantial increases in VEC $[Ca^{2+}]_i$ in the pial and penetrating arteries (PiA and PeA, green arrows) in the brain (**A**) and in glomerular (**G**) capillaries in the kidney (**B**). The right panels show the statistical summary of VEC $[Ca^{2+}]_i$ changes (F_{max}/F_0 , maximal Salsa6f fluorescence intensity normalized to baseline) in response to acute vehicle control or angiotensin II challenge with or without AT₁R or AT₂R inhibitors. A time-lapse video of a similar kidney preparation showing the effects of acute angiotensin II and AT₁Ri+angiotensin II challenge is available in Video S1. **C**, Statistical summary of the hemodynamic effect of acute intracarotid injection of the AT₂R inhibitor PD123319 compared with control in kidney in 2-week-old female mice. **D**, Average RNA expression levels of AT_{1a}R (Agtr1a), AT_{1b}R (Agtr1b), and AT₂R (Agtr2) in rapidly isolated renal vascular endothelial cells. Data points represent the mean expression levels of gene as counts per million transcripts in renal VECs where each data point represents an individual animal. **E**, Comparison analysis of the effects of acute angiotensin II challenge on VEC $[Ca^{2+}]_i$ in brain vs kidney microvessels. **F**, Time course analysis of the effects of acute angiotensin II challenge (illustrated by a dashed vertical line) on VEC $[Ca^{2+}]_i$ and hemodynamic parameters. Representative simultaneous recording of changes in VEC Salsa6f signal (red) and vascular diameter (black) in the same AA over time (left). Note that the peak of Salsa6f fluorescence intensity preceded vasoconstriction which was indicated by the decrease in AA diameter. Representative intravital MPM image of a Sox2–Salsa6f mouse kidney with a glomerulus (**G**) and its adjacent AA that illustrates the simultaneous measurement of $[Ca^{2+}]_i$ in VECs and VSMCs (center). Representative simultaneous recording of the changes in Salsa6f fluorescence intensity in response to acute angiotensin II challenge in VECs (green) and VSMCs (blue) over time. Note that the peak of Salsa6f intensity in a VEC preceded that of a directly adjacent VSMC. **G**, Representative pseudocolor DAF-FM fluorescence intensity images in brain (top) and kidney (bottom) microvessels at baseline and 5 minutes after intracarotid bolus angiotensin II injection of the exact same tissue volume. Note the robust increases in VEC NO production in PiA and PeA in the brain, and in glomerular capillaries (**G**) in the kidney indicated by the yellow-red vs blue colors. The right panels show the statistical summary of the changes in DAF-FM fluorescence intensity in VECs in mouse brain (top) and kidney (bottom) microvessels. Each data point in the graphs corresponds to an average of n=10 measurements/vessel and n=10 different vessels/animal in n=8 mice (4 males [blue] and 4 females [red]) in both groups. * $P < 0.05$ —**** $P < 0.0001$ by 1-way ANOVA (between multiple groups) with Kruskal–Wallis test and unpaired Student's *t* test (between 2 groups). Bars are 50 μ m. AA indicates afferent arteriole; AngII, angiotensin II; AT₁R, type 1 angiotensin II receptor; AT₂R, type 2 angiotensin II receptor; $[Ca^{2+}]_i$, intracellular calcium; DAF-FM, 4-amino-5-methylamino-2',7'-difluorofluorescein diacetate; EA, efferent arteriole; MPM, multiphoton microscopy; NO, nitric oxide; ns, not significant; PeA, penetrating artery; PiA, pial artery; VEC, vascular endothelial cell; and VSMC, vascular smooth muscle cell.

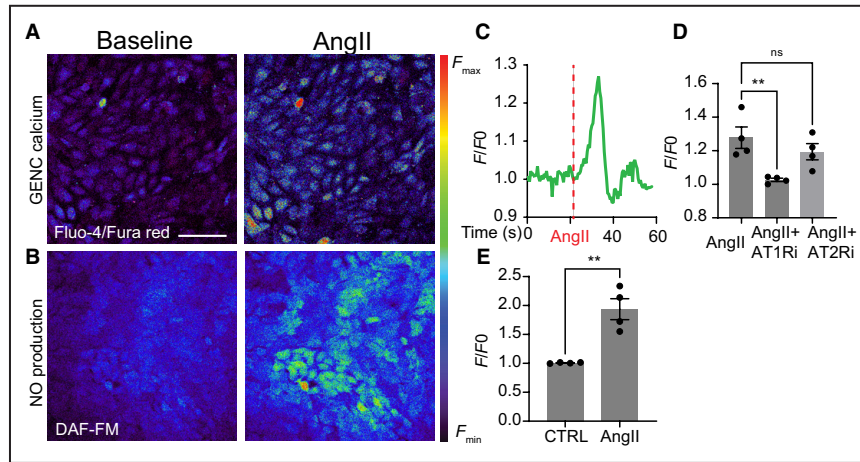


Figure 3. The effects of angiotensin II on calcium signaling and NO production of GEnCs cultured in vitro.

A and B, Representative pseudocolor images of Fluo-4/Fura red and DAF-FM fluorescence intensity (F/F_0) reflecting changes in $[Ca^{2+}]_i$ and NO production, respectively, in GEnCs before and after acute angiotensin II administration (10^{-9} mol/L). Note the increased Fluo-4/Fura red intensity ratio indicated by the appearance of green, yellow, and red pseudocolor cells in response to angiotensin II treatment, in contrast to blue cells at baseline. **C,** Representative recording of the changes in Fluo-4/Fura red fluorescence intensity (full frame) over time. The time of angiotensin II addition is indicated by the vertical red dashed line. **D,** Statistical summary of the angiotensin II-induced changes in GEnC $[Ca^{2+}]_i$ (Fluo-4/Fura red ratio normalized to baseline) with or without pretreatment with the AT_1R inhibitor losartan or the AT_2R inhibitor PD123319. **E,** Statistical summary of the angiotensin II-induced changes in GEnC NO production (DAF-FM fluorescence normalized to baseline). Data points represent the average of 4 full frame measurements in $n=4$ wells each. $**P<0.01$ by 1-way ANOVA (between multiple groups) with Dunnett's multiple comparisons test and unpaired Student's t test (between 2 groups). Bars are $50\mu m$. AngII indicates angiotensin II; AT_1R , type 1 angiotensin II receptor; AT_2R , type 2 angiotensin II receptor; $[Ca^{2+}]_i$, intracellular calcium; Cdh5, cadherin 5; CTRL, control; DAF-FM, 4-amino-5-methylamino-2',7'-difluorofluorescein diacetate; GenC, glomerular endothelial cell; NO, nitric oxide; ns, not significant; and UO, unilateral ureteral obstruction.

(Figure 2D) provides more detailed mouse-specific mechanistic insights and suggests the importance of the AT_{1a} receptor in the present angiotensin II-induced VEC responses. Most transgenic mouse studies using AT_{1a} , AT_{1b} , and AT_2 receptor knockout animals showed that $AT_{1a}R$ is the receptor that drives most physiological responses to angiotensin II including blood pressure control,^{48,49} although other studies underscored the tissue-specific roles of $AT_{1b}R$.⁵⁰ The lack of hypertension in VEC specific $AT_{1a}R$ knock out mice^{51,52} is somewhat conflicting with our results which can be explained by the more pronounced role of this vasodilator mechanism in stressed disease conditions compared with healthy conditions. Angiotensin II-induced VEC calcium responses were exclusively mediated via the AT_1R , in agreement with earlier studies showing that acute vasoconstrictor responses to angiotensin II were mediated by actions at the AT_1R , and that acute responses are not counterbalanced by opposing effects on the AT_2R .⁵³ Other studies provided additional confirmation regarding the key role of the AT_1R and that the AT_2R does not contribute significantly to the

observed angiotensin II-induced VEC calcium elevations or other vascular responses^{54,55} including in brain microvessels.⁵⁶ Our results are also in agreement with the previous demonstration of AT_1R -mediated activation of VEC calcium signaling and NO production by angiotensin II,^{18,19} which has been previously attributed to AT_2R functions.⁵⁷ However, the results of the present study conflict with the earlier observations showing that angiotensin II via the AT_1R attenuates NO production and endothelium-dependent vasodilatation.²² One possible explanation for this discrepancy may reside in the use of in vitro cell and isolated arteriole preparations in that earlier study.²² By demonstrating the direct and positive calcium and NO signaling effects of AT_1R in VECs in vivo, the present study challenges the existing paradigm regarding the generally vasoconstrictor role of the AT_1R , which is clearly context and cell/tissue type dependent.

The findings of higher vasoactive potency of angiotensin II on the endothelium in kidney versus brain microvessels (Figure 2E) and its reduced efficacy in organ disease and hypertension conditions

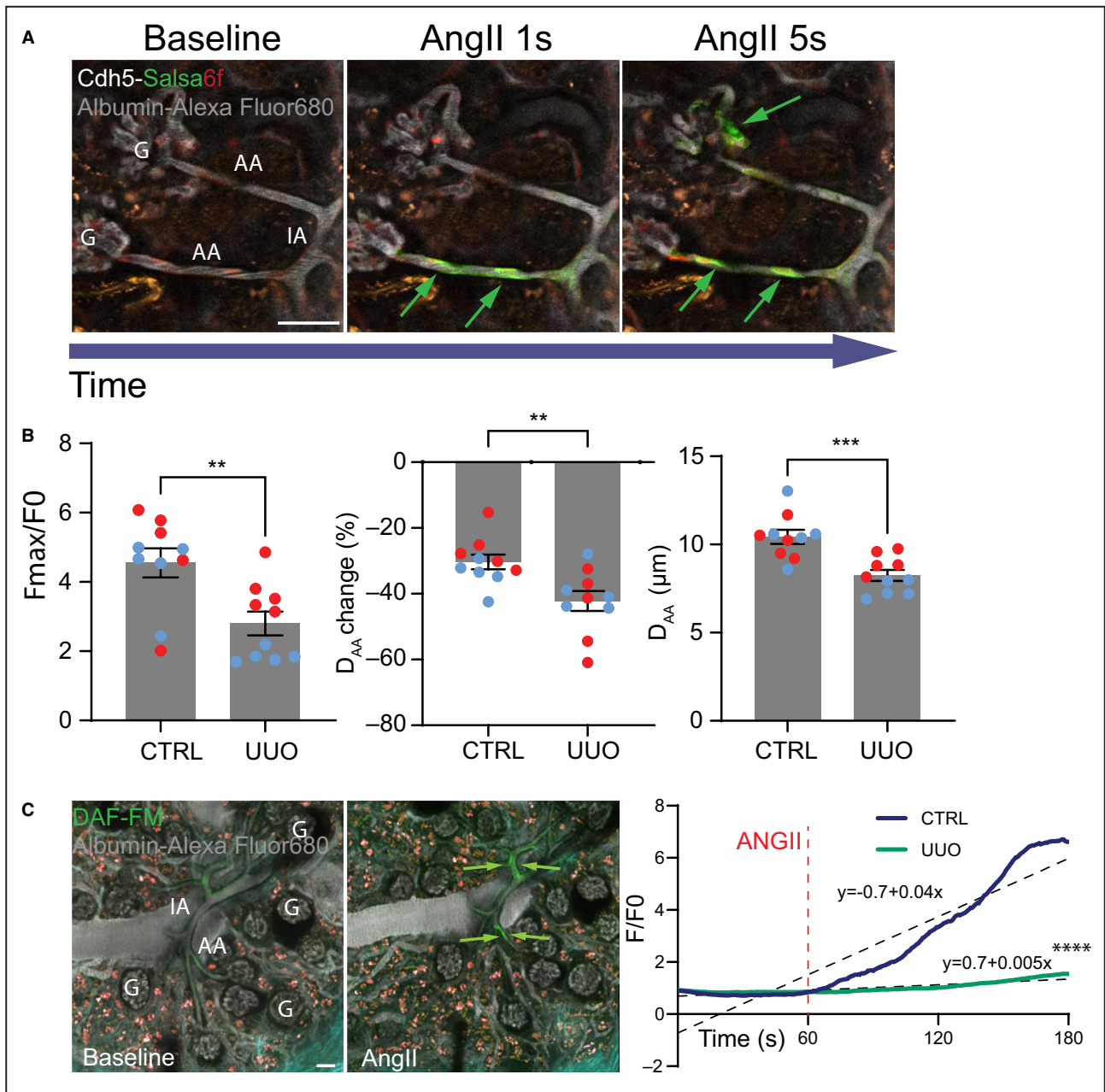
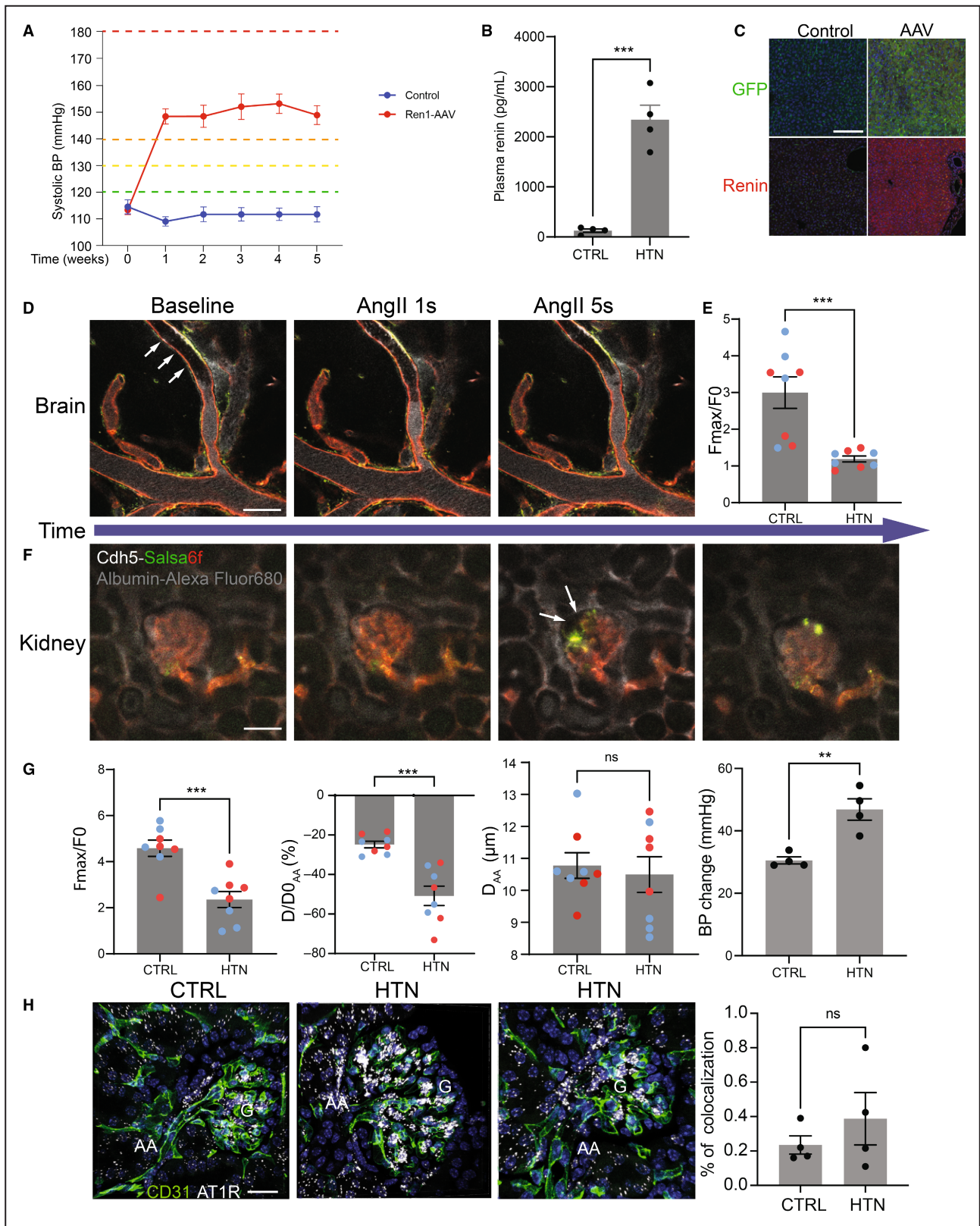


Figure 4. Diminished effects of angiotensin II on VEC calcium signaling and NO production in kidney fibrosis.

A, Representative in vivo MPM images of a cadherin 5–Salsa6f mouse kidney 5 weeks after UUO demonstrating the effects of acute systemic angiotensin II injections (400ng/kg IC in bolus) on VEC $[Ca^{2+}]_i$. Note the increased Salsa6f fluorescence intensity (green arrows) within 1 seconds of angiotensin II injection, indicating increased VEC $[Ca^{2+}]_i$. The circulating plasma was labeled by iv. injected Alexa Fluor 680-conjugated albumin (greyscale). Tissue autofluorescence is shown in orange. **B**, Statistical summary of the angiotensin II–induced changes in Salsa6f fluorescence intensity (F_{max}/F_0) indicating $[Ca^{2+}]_i$ changes in VECs (left) and in the normalized (% of baseline, center) and actual AA diameter (right). Each data point in the graphs correspond to an average of ten measurements/vessel and ten different vessels/animal in $n=8$ mice (4 males (blue) and 4 females (red)) in both groups. $*P<0.05$ – $****P<0.0001$ by unpaired Student’s t test. **C**, Representative in vivo MPM tile scan images of the same area of a UUO mouse kidney before (baseline) and after acute systemic angiotensin II injection (left). VECs were loaded with the NO-sensitive green fluorescent dye DAF-FM to measure VEC NO production. Note the increased DAF-FM fluorescence intensity in AA-IA resistance arterioles but not in glomerular capillaries. Tissue autofluorescence shown in orange. Second harmonic generation signal is shown in cyan. Representative recordings of the baseline and initial rate of the angiotensin II–induced increase in DAF-FM fluorescence intensity in control healthy (blue line) and UUO conditions (green line). $****P<0.0001$ by simple linear regression. $n=4$, 2 male and 2 female mice each. Bars are $50\mu m$. AA indicates afferent arteriole; AngII, angiotensin II; $[Ca^{2+}]_i$, intracellular calcium; Cdh5, cadherin 5; CTRL, control; DAF-FM, 4-amino-5-methylamino-2',7'-difluorofluorescein diacetate; G, glomerulus; HTN, hypertensive mice; IA, interlobular arteriole; NO, nitric oxide; ns, not significant; UUO, unilateral ureteral obstruction; and VEC, vascular endothelial cell.



(Figures 4B and 5G) are consistent with the critical role of the kidney in the pathogenesis of hypertension and its cardiovascular complications.^{58,59} In

the well-established UUO model of kidney fibrosis and high angiotensin II vasoconstrictor state,⁶⁰ as well as in the Ren1-AAV model of renin-angiotensin

Figure 5. Diminished effects of angiotensin II on VEC calcium signaling and NO production in hypertension.

A, Statistical summary of the changes in systolic blood pressure over time in control GFP-AAV injected (blue) or Ren1-AAV-injected hypertensive mice (red). Green-yellow-orange-red horizontal dashed lines illustrate the normal–elevated–stage 1–stage 2 American Heart Association scales of high blood pressure, respectively. **B**, Statistical summary of plasma renin concentrations in control and Ren1-AAV hypertensive mice. N=4 male mice each. **C**, Representative GFP (green) and renin (red) immunofluorescence images of mouse liver sections from control uninjected (left) and either control GFP-AAV-injected (top) or Ren1-AAV-injected mice (bottom right). Note the expression of GFP (green) or renin (red) in hepatocytes of control GFP-AAV or Ren1-AAV-injected mice confirming successful gene delivery. **D** through **F**, Representative in vivo MPM images of intact mouse brain (**D**) and kidney (**F**) microvasculature in a cadherin 5–Salsa6f Ren1-AAV hypertensive mouse. VECs are labeled by the genetic expression of GCaMP6f (green) linked to tdTomato (red). The circulating plasma was labeled by iv. injected Alexa Fluor 680-conjugated albumin (grayscale). Note the relatively small angiotensin II-induced elevations in VEC $[Ca^{2+}]_i$ (GCaMP6f intensity, green), shedding single-cell VECs with high $[Ca^{2+}]_i$ (high GCaMP6f green intensity cells) in glomerular capillaries, and the appearance of several, plasma-excluding microthrombi (black) in both brain and kidney microvessels (arrows). Time-lapse video of the same preparation is available in Video S2. **E**, Statistical summary of acute angiotensin II-induced changes in VEC $[Ca^{2+}]_i$ (Salsa6f fluorescence intensity normalized to baseline) in control healthy and hypertensive mice. **G**, Statistical summary of the angiotensin II-induced changes in Salsa6f fluorescence intensity normalized to baseline indicating $[Ca^{2+}]_i$ changes in VECs (left), normalized (% of baseline) and actual AA diameter, and acute blood pressure (right) in control healthy and hypertensive mice. N=4–8 mice (4 males [blue] and 4 females [red]). Each data point represents an average of 10 measurements. **H**, Representative images and statistical summary of AT₁R mRNA expression (gray) in VECs labeled with CD31 immunostaining (green). Nuclei were labeled blue with 4',6-diamidino-2-phenylindole. (N=4 mice). Bars are 50 μm. ***P*<0.01, ****P*<0.001 by unpaired Student's *t* test. AA indicates afferent arteriole; AAV, adeno-associated virus; AngII, angiotensin II; AT₁R, type 1 angiotensin II receptor; $[Ca^{2+}]_i$, intracellular calcium; CTRL, control; G, glomerulus; GCaMP, calcium sensitive green fluorescent protein analog; GFP, green fluorescent protein; HTN, hypertensive mice; ns, not significant; and VEC, vascular endothelial cell.

system-dependent hypertension,^{28,29} angiotensin II-induced VEC calcium signaling and NO synthesis were significantly reduced compared with healthy control (Figures 4 and 5). These results suggest that diminished agonist-induced VEC calcium signaling and NO production are key mechanisms in the development of vascular and endothelial dysfunction in these disease conditions. Regarding the molecular mechanism, the unaltered expression of AT₁R in VECs (Figure 5H) suggests that the difference in endothelial response in diseased versus healthy mice is not due to altered AT₁R density. Rather, sustained high angiotensin II states are known to cause endothelial dysfunction via multiple mechanisms and signaling cascades that include increased production of reactive oxygen species, reduced NO bioavailability, oxidative stress, and inflammation.^{1,61,62} NO has well-established antithrombotic effects,⁶³ and it also functions as an endothelial cell survival factor.⁶⁴ Therefore, microthrombi formation and VEC shedding observed in the hypertension model (Figure 5F and Video S2) are further consistent with insufficient NO production and endothelial dysfunction in disease conditions (Figures 4B and 4C, 5E). More preserved agonist-induced VEC $[Ca^{2+}]_i$ responses in female versus male UUO and hypertensive mice (Figures 4B and 5G) are consistent with the generally recognized sex and gender differences in cardiovascular and renal diseases.⁶⁵ Our results show larger blood pressure elevations in response to intracoronary bolus angiotensin II injection in hypertensive animals compared with controls (Figure 5G). These results along with the more robust small artery vasoconstriction in hypertensive animals versus controls indicate that the reduced direct angiotensin II effect on VEC calcium in

hypertension plays an important role in the development of hypertension itself and its end-organ complications. (Figure 5D and 5F, Video S2). Importantly, the endothelial calcium responses preceded vasoconstrictions and blood pressure elevations (Figure 2F). Therefore, the altered VECs calcium response is a cause or contributing factor rather than the consequence of the altered blood pressure response in hypertensive animals.

In summary, the present study established and applied new intravital imaging research tools and approaches to specifically study endothelial mechanisms of vascular functions and blood flow regulation in vivo. Direct visualization of the robust angiotensin II-induced elevations in VEC calcium and NO in brain and kidney microvessels confirmed the existence of this vasodilatory mechanism that helps to counterbalance vasoconstriction and maintain residual organ blood flow. Insufficiency of this mechanism was captured in disease conditions and linked to endothelial dysfunction and the development of vascular pathologies.

ARTICLE INFORMATION

Received February 10, 2024; accepted April 15, 2024.

Affiliations

Department of Physiology and Neuroscience, University of Southern California, Los Angeles, CA (A.B.C., U.N.S., S.D., A.I., G.T., A.A.M., J.P., G.G.); Zilkha Neurogenetic Institute, University of Southern California, Los Angeles, CA (A.B.C., U.N.S., S.D., A.I., G.T., J.P., G.G.); and Department of Medicine, University of Southern California, Los Angeles, CA (S.B.G., J.W.N., J.P.).

Acknowledgments

The authors thank Ralf Adams, Cancer Research UK Scientist, for providing cadherin 5 (PAC)-Cre-ERT2 mice via Cancer Research Technology Limited.

Drs Gyarmati and Peti-Peterdi designed the study and wrote the manuscript. Alejandra Becerra Calderon, Sachin Deepak, Audrey Izuhara, Greta Trogen, Urvi Nikhil Shroff, Alicia A. McDonough, Susan B. Gurley, and Jonathan W. Nelson made primary and substantial contributions to acquiring, analyzing, and interpreting data. All authors approved the final version of the manuscript.

Sources of Funding

This work was supported by a Carl W. Gottschalk Research Scholar Grant by the American Society of Nephrology and a Dean's pilot funding award from the Keck School of Medicine at the University of Southern California to Dr Gyarmati, and by US National Institutes of Health grants DK064324, DK123564, and S10OD021833 to Dr Peti-Peterdi.

Disclosures

None.

Supplemental Material

Video S1

Video S2

REFERENCES

- Forrester SJ, Booz GW, Sigmund CD, Coffman TM, Kawai T, Rizzo V, Scalia R, Eguchi S. Angiotensin II signal transduction: an update on mechanisms of physiology and pathophysiology. *Physiol Rev*. 2018;98:1627–1738. doi: [10.1152/physrev.00038.2017](https://doi.org/10.1152/physrev.00038.2017)
- Kobori H, Nangaku M, Navar LG, Nishiyama A. The intrarenal renin-angiotensin system: from physiology to the pathobiology of hypertension and kidney disease. *Pharmacol Rev*. 2007;59:251–287. doi: [10.1124/pr.59.3.3](https://doi.org/10.1124/pr.59.3.3)
- Lin H, Geurts F, Hassler L, Battle D, Mirabito Colafella KM, Denton KM, Zhuo JL, Li XC, Ramkumar N, Koizumi M, et al. Kidney angiotensin in cardiovascular disease: formation and drug targeting. *Pharmacol Rev*. 2022;74:462–505. doi: [10.1124/pharmrev.120.000236](https://doi.org/10.1124/pharmrev.120.000236)
- Schmidt K, de Wit C. Endothelium-derived hyperpolarizing factor and myoendothelial coupling: the in vivo perspective. *Front Physiol*. 2020;11:602930. doi: [10.3389/fphys.2020.602930](https://doi.org/10.3389/fphys.2020.602930)
- Vanhoutte PM, Zhao Y, Xu A, Leung SW. Thirty years of saying NO: sources, fate, actions, and misfortunes of the endothelium-derived vasodilator mediator. *Circ Res*. 2016;119:375–396. doi: [10.1161/circresaha.116.306531](https://doi.org/10.1161/circresaha.116.306531)
- Tallini YN, Brekke JF, Shui B, Doran R, Hwang SM, Nakai J, Salama G, Segal SS, Kotlikoff MI. Propagated endothelial Ca²⁺ waves and arteriolar dilation in vivo: measurements in Cx40BAC GCaMP2 transgenic mice. *Circ Res*. 2007;101:1300–1309. doi: [10.1161/circresaha.107.149484](https://doi.org/10.1161/circresaha.107.149484)
- Ledoux J, Taylor MS, Bonev AD, Hannah RM, Solodushko V, Shui B, Tallini Y, Kotlikoff MI, Nelson MT. Functional architecture of inositol 1,4,5-trisphosphate signaling in restricted spaces of myoendothelial projections. *Proc Natl Acad Sci USA*. 2008;105:9627–9632. doi: [10.1073/pnas.0801963105](https://doi.org/10.1073/pnas.0801963105)
- Ko Y, Glodny B, Stier S, Totzke G, Nickenig G, Düsing R, Sachinidis A, Vetter H. Angiotensin type-1 (AT1) receptor gene expression in primarily cultured human arterial umbilical endothelial cells. *Biochem Pharmacol*. 1997;53:417–421. doi: [10.1016/s0006-2952\(96\)00691-0](https://doi.org/10.1016/s0006-2952(96)00691-0)
- Peppiatt-Wildman CM, Crawford C, Hall AM. Fluorescence imaging of intracellular calcium signals in intact kidney tissue. *Nephron Exp Nephrol*. 2012;121:e49–e58. doi: [10.1159/000342812](https://doi.org/10.1159/000342812)
- Gyarmati G, Jacob CO, Peti-Peterdi J. New endothelial mechanisms in glomerular (Patho)biology and proteinuria development captured by intravital multiphoton imaging. *Front Med (Lausanne)*. 2021;8:765356. doi: [10.3389/fmed.2021.765356](https://doi.org/10.3389/fmed.2021.765356)
- Gyarmati G, Shroff UN, Izuhara A, Hou X, Da Sacco S, Sedrakyan S, Lemley KV, Amann K, Perin L, Peti-Peterdi J. Intravital imaging reveals glomerular capillary distension and endothelial and immune cell activation early in Alport syndrome. *JCI Insight*. 2022;7:7. doi: [10.1172/jci.insight.152676](https://doi.org/10.1172/jci.insight.152676)
- Desposito D, Schiessi IM, Gyarmati G, Riquier-Brison A, Izuhara AK, Kadoya H, Der B, Shroff UN, Hong YK, Peti-Peterdi J. Serial intravital imaging captures dynamic and functional endothelial remodeling with single-cell resolution. *JCI Insight*. 2021;6:6. doi: [10.1172/jci.insight.123392](https://doi.org/10.1172/jci.insight.123392)
- Gyarmati G, Toma I, Izuhara A, Burford JL, Shroff UN, Papadouri S, Deepak S, Peti-Peterdi J. The role of TRPC6 calcium channels and P2 purinergic receptors in podocyte mechanical and metabolic sensing. *Physiol Int*. 2021;109:31–45. doi: [10.1556/2060.2021.00205](https://doi.org/10.1556/2060.2021.00205)
- Pueyo ME, Michel JB. Angiotensin II receptors in endothelial cells. *Gen Pharmacol*. 1997;29:691–696. doi: [10.1016/s0306-3623\(97\)00021-9](https://doi.org/10.1016/s0306-3623(97)00021-9)
- Ramchandran R, Takezako T, Saad Y, Stull L, Fink B, Yamada H, Dikalov S, Harrison DG, Moravec C, Karnik SS. Angiotensinergic stimulation of vascular endothelium in mice causes hypotension, bradycardia, and attenuated angiotensin response. *Proc Natl Acad Sci USA*. 2006;103:19087–19092. doi: [10.1073/pnas.0602715103](https://doi.org/10.1073/pnas.0602715103)
- Aiken JW, Vane JR. Intrarenal prostaglandin release attenuates the renal vasoconstrictor activity of angiotensin. *J Pharmacol Exp Ther*. 1973;184:678–687.
- Schlondorff D, Rocznik S, Satriano JA, Folkert VW. Prostaglandin synthesis by isolated rat glomeruli: effect of angiotensin II. *Am J Physiol*. 1980;239:F486–F495. doi: [10.1152/ajprenal.1980.239.5.F486](https://doi.org/10.1152/ajprenal.1980.239.5.F486)
- Pueyo ME, Arnal JF, Rami J, Michel JB. Angiotensin II stimulates the production of NO and peroxynitrite in endothelial cells. *Am J Physiol*. 1998;274:C214–C220. doi: [10.1152/ajpcell.1998.274.1.C214](https://doi.org/10.1152/ajpcell.1998.274.1.C214)
- Suzuki H, Eguchi K, Ohtsu H, Higuchi S, Dhobale S, Frank GD, Motley ED, Eguchi S. Activation of endothelial nitric oxide synthase by the angiotensin II type 1 receptor. *Endocrinology*. 2006;147:5914–5920. doi: [10.1210/en.2006-0834](https://doi.org/10.1210/en.2006-0834)
- Boulanger CM, Caputo L, Lévy BI. Endothelial AT1-mediated release of nitric oxide decreases angiotensin II contractions in rat carotid artery. *Hypertension*. 1995;26:752–757. doi: [10.1161/01.hyp.26.5.752](https://doi.org/10.1161/01.hyp.26.5.752)
- Fleming I. Molecular mechanisms underlying the activation of eNOS. *Pflugers Arch*. 2010;459:793–806. doi: [10.1007/s00424-009-0767-7](https://doi.org/10.1007/s00424-009-0767-7)
- Loot AE, Schreiber JG, Fisslthaler B, Fleming I. Angiotensin II impairs endothelial function via tyrosine phosphorylation of the endothelial nitric oxide synthase. *J Exp Med*. 2009;206:2889–2896. doi: [10.1084/jem.20090449](https://doi.org/10.1084/jem.20090449)
- Emori T, Hirata Y, Ohta K, Kanno K, Eguchi S, Imai T, Shichiri M, Marumo F. Cellular mechanism of endothelin-1 release by angiotensin and vasopressin. *Hypertension*. 1991;18:165–170. doi: [10.1161/01.HYP.18.2.165](https://doi.org/10.1161/01.HYP.18.2.165)
- Mehta PK, Griendling KK. Angiotensin II cell signaling: physiological and pathological effects in the cardiovascular system. *Am J Physiol Cell Physiol*. 2007;292:C82–C97. doi: [10.1152/ajpcell.00287.2006](https://doi.org/10.1152/ajpcell.00287.2006)
- Wang Y, Nakayama M, Pitulescu ME, Schmidt TS, Bochenek ML, Sakakibara A, Adams S, Davy A, Deutsch U, Lüthi U, et al. Ephrin-B2 controls VEGF-induced angiogenesis and lymphangiogenesis. *Nature*. 2010;465:483–486. doi: [10.1038/nature09002](https://doi.org/10.1038/nature09002)
- Dong TX, Othy S, Jairaman A, Skupsky J, Zavala A, Parker I, Dynes JL, Cahalan MD. T-cell calcium dynamics visualized in a ratiometric tdTomato-GCaMP6f transgenic reporter mouse. *eLife*. 2017;6:6. doi: [10.7554/eLife.32417](https://doi.org/10.7554/eLife.32417)
- Hayashi S, Lewis P, Pevny L, McMahon AP. Efficient gene modulation in mouse epiblast using a Sox2Cre transgenic mouse strain. *Mech Dev*. 2002;119(suppl 1):S97–s101. doi: [10.1016/s0925-4773\(03\)00099-6](https://doi.org/10.1016/s0925-4773(03)00099-6)
- Caron KM, James LR, Kim HS, Morham SG, Sequeira Lopez ML, Gomez RA, Reudelhuber TL, Smithies O. A genetically clamped renin transgene for the induction of hypertension. *Proc Natl Acad Sci USA*. 2002;99:8248–8252. doi: [10.1073/pnas.112222199](https://doi.org/10.1073/pnas.112222199)
- Harlan SM, Ostroski RA, Coskun T, Yantis LD, Breyer MD, Heuer JG. Viral transduction of renin rapidly establishes persistent hypertension in diverse murine strains. *Am J Physiol Regul Integr Comp Physiol*. 2015;309:R467–R474. doi: [10.1152/ajpregu.00106.2015](https://doi.org/10.1152/ajpregu.00106.2015)
- Østergaard MV, Secher T, Christensen M, Salinas CG, Roostalu U, Skytte JL, Rune I, Hansen HH, Jelsing J, Vrang N, et al. Therapeutic effects of lisinopril and empagliflozin in a mouse model of hypertension-accelerated diabetic kidney disease. *Am J Physiol Renal Physiol*. 2021;321:F149–F161. doi: [10.1152/ajprenal.00154.2021](https://doi.org/10.1152/ajprenal.00154.2021)
- Riquier-Brison ADM, Sipos A, Prókai Á, Vargas SL, Toma L, Meer EJ, Villanueva KG, Chen JCM, Gyarmati G, Yih C, et al. The macula densa prerenin receptor is essential in renin release and blood pressure control. *Am J Physiol Renal Physiol*. 2018;315:F521–F534. doi: [10.1152/ajprenal.00029.2018](https://doi.org/10.1152/ajprenal.00029.2018)
- Hackl MJ, Burford JL, Villanueva K, Lam L, Suszták K, Schermer B, Benzing T, Peti-Peterdi J. Tracking the fate of glomerular epithelial cells in vivo using serial multiphoton imaging in new mouse models with fluorescent lineage tags. *Nat Med*. 2013;19:1661–1666. doi: [10.1038/nm.3405](https://doi.org/10.1038/nm.3405)

33. Kang JJ, Toma I, Sipos A, McCulloch F, Peti-Peterdi J. Quantitative imaging of basic functions in renal (patho)physiology. *Am J Physiol Renal Physiol*. 2006;291:F495–F502. doi: [10.1152/ajprenal.00521.2005](https://doi.org/10.1152/ajprenal.00521.2005)
34. Kisler K, Nelson AR, Rege SV, Ramanathan A, Wang Y, Ahuja A, Lasic D, Tsai PS, Zhao Z, Zhou Y, et al. Pericyte degeneration leads to neurovascular uncoupling and limits oxygen supply to brain. *Nat Neurosci*. 2017;20:406–416. doi: [10.1038/nn.4489](https://doi.org/10.1038/nn.4489)
35. Terpolilli NA, Kim SW, Thal SC, Kataoka H, Zeisig V, Nitzsche B, Klaesner B, Zhu C, Schwarzmaier S, Meissner L, et al. Inhalation of nitric oxide prevents ischemic brain damage in experimental stroke by selective dilatation of collateral arterioles. *Circ Res*. 2012;110:727–738. doi: [10.1161/circresaha.111.253419](https://doi.org/10.1161/circresaha.111.253419)
36. Bekendam RH, Iyu D, Passam F, Stopa JD, De Ceunynck K, Muse O, Bendapudi PK, Garnier CL, Gopal S, Crescence L, et al. Protein disulfide isomerase regulation by nitric oxide maintains vascular quiescence and controls thrombus formation. *J Thromb Haemost*. 2018;16:2322–2335. doi: [10.1111/jth.14291](https://doi.org/10.1111/jth.14291)
37. Endres BT, Staruschenko A, Schulte M, Geurts AM, Palygin O. Two-photon imaging of intracellular Ca²⁺ handling and nitric oxide production in endothelial and smooth muscle cells of an isolated rat aorta. *J Vis Exp*. 2015:e52734. doi: [10.3791/52734](https://doi.org/10.3791/52734)
38. Toma I, Bansal E, Meer EJ, Kang JJ, Vargas SL, Peti-Peterdi J. Connexin 40 and ATP-dependent intercellular calcium wave in renal glomerular endothelial cells. *Am J Physiol Regul Integr Comp Physiol*. 2008;294:R1769–R1776. doi: [10.1152/ajpregu.00489.2007](https://doi.org/10.1152/ajpregu.00489.2007)
39. Kovács G, Komlósi P, Fuson A, Peti-Peterdi J, Rosivall L, Bell PD. Neuronal nitric oxide synthase: its role and regulation in macula densa cells. *J Am Soc Nephrol*. 2003;14:2475–2483. doi: [10.1097/01.asn.0000088737.05283.2b](https://doi.org/10.1097/01.asn.0000088737.05283.2b)
40. Akgür FM, Zibari GB, McDonald JC, Granger ND, Brown MF. Kinetics of P-selectin expression in regional vascular beds after resuscitation of hemorrhagic SHOCK: a clue to the mechanism of multiple system organ failure. *Shock*. 2000;13:140–144. doi: [10.1097/00024382-200013020-00008](https://doi.org/10.1097/00024382-200013020-00008)
41. Pluznick JL, Protzko RJ, Gevorgyan H, Peterlin Z, Sipos A, Han J, Brunet I, Wan LX, Rey F, Wang T, et al. Olfactory receptor responding to gut microbiota-derived signals plays a role in renin secretion and blood pressure regulation. *Proc Natl Acad Sci USA*. 2013;110:4410–4415. doi: [10.1073/pnas.1215927110](https://doi.org/10.1073/pnas.1215927110)
42. Scarfe L, Schock-Kusch D, Ressel L, Friedemann J, Shulhevich Y, Murray P, Wilm B, de Caestecker M. Transdermal measurement of glomerular filtration rate in mice. *J Vis Exp*. 2018;21:e58520. doi: [10.3791/58520](https://doi.org/10.3791/58520)
43. Gyarmati G, Shroff UN, Riquier-Brison A, Kriz W, Kaissling B, Neal CR, Arkill KP, Ahmadi N, Gill IS, Moon JY, et al. A new view of macula densa cell microanatomy. *Am J Physiol Renal Physiol*. 2021;320:F492–f504. doi: [10.1152/ajprenal.00546.2020](https://doi.org/10.1152/ajprenal.00546.2020)
44. Emechebe U, Nelson JW, Alkayed NJ, Kaul S, Adey AC, Barnes AP. Age-dependent transcriptional alterations in cardiac endothelial cells. *Physiol Genomics*. 2021;53:295–308. doi: [10.1152/physiolgenomics.00037.2021](https://doi.org/10.1152/physiolgenomics.00037.2021)
45. Sampson AK, Moritz KM, Denton KM. Postnatal ontogeny of angiotensin receptors and ACE2 in male and female rats. *Gen Med*. 2012;9:21–32. doi: [10.1016/j.genm.2011.12.003](https://doi.org/10.1016/j.genm.2011.12.003)
46. Iekushi K, Taniyama Y, Kusunoki H, Azuma J, Sanada F, Okayama K, Koibuchi N, Iwabayashi M, Rakugi H, Morishita R. Hepatocyte growth factor attenuates transforming growth factor- β -angiotensin II crosstalk through inhibition of the PTEN/AKT pathway. *Hypertension*. 2011;58:190–196. doi: [10.1161/hypertensionaha.111.173013](https://doi.org/10.1161/hypertensionaha.111.173013)
47. Meng L, Wang Y, Zhang L, McDonagh DL. Heterogeneity and variability in pressure autoregulation of organ blood flow: lessons learned over 100+ years. *Crit Care Med*. 2019;47:436–448. doi: [10.1097/ccm.00000000000003569](https://doi.org/10.1097/ccm.00000000000003569)
48. Emathingier JM, Nelson JW, Gurley SB. Advances in use of mouse models to study the renin-angiotensin system. *Mol Cell Endocrinol*. 2021;529:111255. doi: [10.1016/j.mce.2021.111255](https://doi.org/10.1016/j.mce.2021.111255)
49. van Esch JH, Gembardt F, Sterner-Kock A, Heringer-Walther S, Le TH, Lassner D, Stijnen T, Coffman TM, Schultheiss HP, Danser AH, et al. Cardiac phenotype and angiotensin II levels in AT1a, AT1b, and AT2 receptor single, double, and triple knockouts. *Cardiovasc Res*. 2010;86:401–409. doi: [10.1093/cvr/cvq004](https://doi.org/10.1093/cvr/cvq004)
50. Zhou Y, Dirksen WP, Chen Y, Morris M, Zweier JL, Periasamy M. A major role for AT1b receptor in mouse mesenteric resistance vessels and its distribution in heart and neuroendocrine tissues. *J Mol Cell Cardiol*. 2005;38:693–696. doi: [10.1016/j.yjmcc.2005.02.009](https://doi.org/10.1016/j.yjmcc.2005.02.009)
51. Rateri DL, Moorleghen JJ, Balakrishnan A, Owens AP 3rd, Howatt DA, Subramanian V, Poduri A, Charnigo R, Cassis LA, Daugherty A. Endothelial cell-specific deficiency of ang II type 1a receptors attenuates ang II-induced ascending aortic aneurysms in LDL receptor^{-/-} mice. *Circ Res*. 2011;108:574–581. doi: [10.1161/circresaha.110.222844](https://doi.org/10.1161/circresaha.110.222844)
52. Poduri A, Rateri DL, Howatt DA, Balakrishnan A, Moorleghen JJ, Cassis LA, Daugherty A. Fibroblast angiotensin II type 1a receptors contribute to angiotensin II-induced medial hyperplasia in the ascending aorta. *Arterioscler Thromb Vasc Biol*. 2015;35:1995–2002. doi: [10.1161/atvbaha.115.305995](https://doi.org/10.1161/atvbaha.115.305995)
53. Bivalacqua TJ, Champion HC, Hyman AL, McNamara DB, Kadowitz PJ. Analysis of responses to angiotensin II in the mouse. *J Renin-Angiotensin-Aldosterone Syst*. 2001;2:S48–s53. doi: [10.1177/14703203010020010801](https://doi.org/10.1177/14703203010020010801)
54. Jacques D, Abdel-Karim Abdel-Malak N, Abou Abdallah N, Al-Khoury J, Bkaily G. Difference in the response to angiotensin II between left and right ventricular endocardial endothelial cells. *Can J Physiol Pharmacol*. 2017;95:1271–1282. doi: [10.1139/cjpp-2017-0280](https://doi.org/10.1139/cjpp-2017-0280)
55. Kamal M, Jacques D, Bkaily G. Angiotensin II receptors' modulation of calcium homeostasis in human vascular endothelial cells. *Can J Physiol Pharmacol*. 2017;95:1289–1297. doi: [10.1139/cjpp-2017-0416](https://doi.org/10.1139/cjpp-2017-0416)
56. Fleegal-DeMotta MA, Doghu S, Banks WA. Angiotensin II modulates BBB permeability via activation of the AT(1) receptor in brain endothelial cells. *J Cereb Blood Flow Metab*. 2009;29:640–647. doi: [10.1038/jcbfm.2008.158](https://doi.org/10.1038/jcbfm.2008.158)
57. Peluso AA, Bertelsen JB, Andersen K, Mortensen TP, Hansen PB, Sumners C, Bader M, Santos RA, Steckelings UM. Identification of protein phosphatase involvement in the AT(2) receptor-induced activation of endothelial nitric oxide synthase. *Clin Sci (Lond)*. 2018;132:777–790. doi: [10.1042/cs20171598](https://doi.org/10.1042/cs20171598)
58. Crowley SD, Coffman TM. In hypertension, the kidney rules. *Curr Hypertens Rep*. 2007;9:148–153. doi: [10.1007/s11906-007-0026-2](https://doi.org/10.1007/s11906-007-0026-2)
59. Crowley SD, Gurley SB, Herrera MJ, Ruiz P, Griffiths R, Kumar AP, Kim HS, Smithies O, Le TH, Coffman TM. Angiotensin II causes hypertension and cardiac hypertrophy through its receptors in the kidney. *Proc Natl Acad Sci USA*. 2006;103:17985–17990. doi: [10.1073/pnas.0605545103](https://doi.org/10.1073/pnas.0605545103)
60. Chevalier RL, Forbes MS, Thornhill BA. Ureteral obstruction as a model of renal interstitial fibrosis and obstructive nephropathy. *Kidney Int*. 2009;75:1145–1152. doi: [10.1038/ki.2009.86](https://doi.org/10.1038/ki.2009.86)
61. Higuchi S, Ohtsu H, Suzuki H, Shirai H, Frank GD, Eguchi S. Angiotensin II signal transduction through the AT1 receptor: novel insights into mechanisms and pathophysiology. *Clin Sci (Lond)*. 2007;112:417–428. doi: [10.1042/cs20060342](https://doi.org/10.1042/cs20060342)
62. Nguyen Dinh Cat A, Montezano AC, Burger D, Touyz RM. Angiotensin II, NADPH oxidase, and redox signaling in the vasculature. *Antioxid Redox Signal*. 2013;19:1110–1120. doi: [10.1089/ars.2012.4641](https://doi.org/10.1089/ars.2012.4641)
63. Versteeg HH, Heemskerk JW, Levi M, Reitsma PH. New fundamentals in hemostasis. *Physiol Rev*. 2013;93:327–358. doi: [10.1152/physrev.00016.2011](https://doi.org/10.1152/physrev.00016.2011)
64. Dimmeler S, Zeiher AM. Nitric oxide—an endothelial cell survival factor. *Cell Death Differ*. 1999;6:964–968. doi: [10.1038/sj.cdd.4400581](https://doi.org/10.1038/sj.cdd.4400581)
65. Reckelhoff JF, Samson WK. Sex and gender differences in cardiovascular, renal and metabolic diseases. *Am J Physiol Regul Integr Comp Physiol*. 2015;309:R1057–R1059. doi: [10.1152/ajpregu.00417.2015](https://doi.org/10.1152/ajpregu.00417.2015)